Published OnlineFirst September 18, 2018; DOI: 10.1158/0008-5472.CAN-18-0707

Translational Science

Cancer Research

Preclinical Evaluation of the Hsp70 Peptide Tracer TPP-PEG_{24}-DFO[^{89}Zr] for Tumor-Specific PET/CT Imaging

Stefan Stangl[1], Lorenzo Tei[2], Francesco De Rose[3], Sybille Reder[3], Jonathan Martinelli[2], Wolfgang Sievert[1], Maxim Shevtsov[1,4,5], Rupert Öllinger[6], Roland Rad[6], Markus Schwaiger[3], Calogero D'Alessandria[3], and Gabriele Multhoff[1]

Abstract

High precision *in vivo* PET/CT imaging of solid tumors improves diagnostic credibility and clinical outcome of patients. An epitope of the oligomerization domain of Hsp70 is exclusively exposed on the membrane of a large variety of tumor types, but not on normal cells, and thus provides a universal tumor-specific target. Here we developed a novel PET tracer TPP-PEG_{24}-DFO[^{89}Zr] based on the tumor cell–penetrating peptide probe TPP, which specifically recognizes membrane Hsp70 (mHsp70) on tumor cells. The implemented PEG_{24} moiety supported tracer stability and improved biodistribution characteristics *in vivo*. The K_d of the tracer ranged in the low nanomolar range (18.9 ± 11.3 nmol/L). Fluorescein isothiocyanate (FITC)-labeled derivatives TPP-[FITC] and TPP-PEG_{24}-[FITC] revealed comparable and specific binding to mHsp70-positive 4T1, 4T1$^+$, a derivative of the 4T1 cell line sorted for high Hsp70 expression, and CT26 tumor cells, but not to mHsp70-negative normal fibroblasts. The rapid internalization kinetics of mHsp70 into the cytosol and the favorable biodistribution of the peptide-based tracer TPP-PEG_{24}-DFO[^{89}Zr] *in vivo* enabled a tumor-specific accumulation with a high tumor-to-background contrast and renal body clearance. The tumor-specific enrichment of the tracer in 4T1$^+$ (6.2 ± 1.1%ID/g), 4T1 (4.3 ± 0.7%ID/g), and CT26 (2.6 ± 0.6%ID/g) mouse tumors with very high, high, and intermediate mHsp70 densities, respectively, reflected mHsp70 expression profiles of the different tumor types, whereas benign mHsp70-negative fibroblastic hyperplasia showed no tracer accumulation (0.2 ± 0.03%ID/g). The ability of our chemically optimized peptide-based tracer TPP-PEG_{24}-DFO[^{89}Zr] to detect mHsp70 *in vivo* suggests its broad applicability in targeting and imaging with high specificity for any tumor type that exhibits surface expression of Hsp70.

Significance: A novel peptide-based PET tracer against the oligomerization domain of Hsp70 has potential for universal tumor-specific imaging *in vivo* across many tumor type. *Cancer Res; 78(21); 6268–81. ©2018 AACR.*

Introduction

The search for suitable PET tracers for tumor-specific detection has always been a research area in molecular imaging. Diagnostic tumor tracers for specific detection of tumors in early stages and monitoring of therapy responses can improve clinical outcome. Clinically applied tracers frequently address metabolic tumor features (e.g., FDG-based tracers; ref. 1) or target molecules that are overexpressed in tumor cells, but are also displayed on the plasma membrane of normal cells. Consequently, these tracers show suboptimal tumor specificity and false positive signals in nonneoplastic tissues (2). Therefore, novel imaging approaches focus on tracers targeting epitopes that are exclusively present on tumor cells. In addition to cancer-related mutational epitopes, *de novo* membrane-bound, tumor targets provide attractive candidates for tumor-specific *in vivo* imaging (3). The membrane-bound form of the major stress-inducible 72 kDa heat shock protein 70 (Hsp70, Hsp70-1, HspA1A; #3303) represents such a tumor-specific target (4). As an important player in the network of other chaperones and cochaperones (5), including Hsp40, Hsp90, HiP, and HoP, Hsp70 is a key player in proteome homeostasis of mammalian cells (6). Hsp70 is expressed in the cytosol of all nucleated cells where it fulfils a variety of chaperoning

[1]Radiation Immuno Oncology Group, Center for Translational Cancer Research (TranslaTUM), Campus Klinikum rechts der Isar, Technische Universität München (TUM), Munich, Germany. [2]Dipartimento di Scienze e Innovazione Tecnologica, Università del Piemonte Orientale "A. Avogadro", Alessandria, Italy. [3]Department of Nuclear Medicine, Klinikum rechts der Isar, Technische Universität München (TUM), Munich, Germany. [4]Institute of Cytology of the Russian Academy of Sciences (RAS), St. Petersburg, Russia. [5]Pavlov First Saint Petersburg State Medical University, St. Petersburg, Russia. [6]Medical Department II, Translational Gastroenterological Oncology, Centre for Translational Cancer Research (TranslaTUM), Klinikum rechts der Isar, Technische Universität München, Munich, Germany.

Note: Supplementary data for this article are available at Cancer Research Online (http://cancerres.aacrjournals.org/).

S. Stangl, L. Tei, C. D'Alessandria, and G. Multhoff contributed equally to this article.

Corresponding Author: Gabriele Multhoff, Center for Translational Cancer Research (TranslaTUM) Campus Klinikum rechts der Isar, Technische Universität München (TUM), Munich 81675, Germany. Phone: 4989-4140-4514; Fax: 4989-4140-4299; E-mail: Gabriele.Multhoff@tum.de

doi: 10.1158/0008-5472.CAN-18-0707

Published OnlineFirst September 18, 2018; DOI: 10.1158/0008-5472.CAN-18-0707

functions, such as folding and assembly of nascent polypeptides, refolding of denatured proteins, as well as regulation of protein transport across membranes. Hsp70-mediated processes require an ATP-dependent transient association of their substrate-binding domain with lipophilic domains of denatured proteins (7). Oligomerization of human Hsp70 is regulated by a domain ($aa_{385–540}$) within the C-terminal substrate-binding domain ($aa_{382–641}$; ref. 5). The majority of human tumors of different entities is characterized by a constitutive overexpression of Hsp70, which supports tumor progression, survival, metastatic spread (8–10), and resistance to therapy (11). In a multicenter clinical trial, we could demonstrate that high intracellular Hsp70 levels at diagnosis predict poor overall survival in patients with squamous cell carcinomas (12). Importantly, we and others could show that, apart from its cytosolic localization, Hsp70 is also present on the plasma membrane of a large variety of different tumor types, but not on normal cells (13–21), and thereby serves as a tumor-specific target. Preclinical therapeutic approaches using cmHsp70.1 mAb for targeting mHsp70 on tumor cells revealed an ample tumor-specific binding *in vivo*, that results in a potent activation of the hosts' antibody-dependent cellular antitumor immune response (21). However, due to the large size (150 kDa) and the immunogenic potential, antibody-based PET probes exhibit certain limitations for imaging purposes including unfavorable biodistribution kinetics caused by long blood circulation times and slow tumor uptake (22), high accumulation in the liver, which increases the risk of hepatoradiotoxicity, and Fc receptor–based off-target effects (23–25). For *in vivo* imaging applications, smaller molecules, such as peptides, show numerous advantages over antibodies including short circulation periods, fast body clearance, favorable biodistribution, improved ingress into solid tumors, and highly efficient tumor cell penetration capabilities (26).

The 14-mer peptide TPP that mimics properties of the oligomerization domain of Hsp70 enables a tumor-specific targeting via mHsp70. As mHsp70 follows a rapid turnover circuit through the endolysosomal pathway (27), TPP peptide subsequently accumulates inside viable, metabolically active, mHsp70-positive tumor cells (28, 29). This tumor-specific uptake increases protection from target clearance and thereby results in a high tumor-to-background ratio, *in vivo*. The tumor specificity of TPP peptide was proven in various, murine syngeneic and human xenograft, endogenous pancreatic ductal adenocarcinoma (PDAC), and spontaneous colitis-induced colon tumor models (29). As a naturally occurring breakdown product of Hsp70, TPP shows an excellent safety and tolerability profile (29), which enables repeated administrations of the tracer. Herein, tumor-specific TPP peptide was applied for the first time as a PET tracer for *in vivo* targeting of mammary and colon tumors in immunocompetent mice.

For *in vivo* PET imaging of tumors, the kinetics of tumor enrichment and biodistribution of a tracer is dependent on both, biochemical characteristics (like molecular size, immunogenicity, binding specificity and affinity, or lipophilicity), as well as on the biological features of the target epitope (among others, membrane density of the epitope, cellular internalization characteristics, intracellular processing of the tracer–target complex). Herein, we characterize a peptide (TPP)-based, 3.5 kDa PET tracer, with a K_d of 18.9 nmol/L and a log*P* value of -3.60 ± 0.2 (TPP-PEG_{24}-DFO[^{89}Zr]). Tumor-specific binding to mHsp70, which is displayed specifically on tumor cells, is mediated by mimicking features of the oligomerization domain of Hsp70. Membrane-bound Hsp70 is characterized by a rapid, endolysosomal internalization pathway, leading to a continuous intercellular accumulation of the tracer over time, *in vitro* and *in vivo*. *In vivo* biodistribution and tumor-specific enrichment of TPP-peptide based tracers in epifluorescence- and PET applications revealed both, tumor-specific enrichment and an optimal tumor-to-background contrast, 24 hours after intravenous administration. With a half-life of 78.4 hours and $E_{\beta+max}$ of 0.9 MeV, Zirconium-89 (^{89}Zr) emits a suitable PET signal at this time-point (30). In addition, the maximum energy emitted by ^{89}Zr (902 KeV) implies that the travel distance of an emitted positron in tissue is relatively short before annihilating. This enables high-resolution images for small target structures like early-stage tumors and metastases. Other positron emitters that are potentially useful for labeling of peptide-based probes, for example, Iodine-124 (^{124}I; t1/2 = 4.2d, $E_{\beta+max}$ 1,532MeV) or Copper-64 (^{64}Cu; t1/2 = 12.7 h, $E_{\beta+max}$ 0.653 MeV), have not been investigated due to the high emitted energy, which can result in a reduced resolution of the PET images. In addition, due to an *in vivo* deiodination effect of ^{124}I during uptake of the tracer and due to the short half-life of ^{64}Cu, which is not matching the distribution kinetics of the Hsp70 targeting peptide-based tracer, we have chosen ^{89}Zr, but not ^{124}I or ^{64}Cu as a radio-emitting isotope.

Chemical properties such as stability, solubility, and biodistribution kinetics of the ^{89}Zr-radiolabeled tracer were optimized by introducing a 24-mer PEG chain to the binding-active TPP moiety, which finally results in TPP-PEG_{24}-DFO[^{89}Zr], according to a method that was described for adjusting *in vivo* biodistribution characteristics (31). Previously, we reported on the application of an Hsp70-targeting, mouse IgG1 mAb for immunotherapy (21) and fluorescence-based imaging (32). In this study, the biodistribution of the monospecific, bivalent binding mAb cmHsp70.1 (K_d = 5.4 nmol/L) equipped with ^{89}Zr by a DFO chelator, was tested. Because of the different sizes of the antibody (150 kDa) and peptide-based Hsp70-targeting tracer (3.5 kDa) with different *in vivo* distribution kinetics, comparability of the biodistribution was approached on the basis of an equal extravasation of the compounds from the vascular system into organs to minimize effects of freely circulating tracers on organ enrichment.

Materials and Methods

Synthesis and radiolabeling of Hsp70-reactive tracers

[FITC]-TKDNNLLGRFELSG-acid (TPP-[FITC]) peptide was purchased from Cambridge Research Biochemicals (UK) at a purity >97%. TPP-PEG_{24}-DFO, TPP-PEG_{24}-DFO[^{nat}Zr], consisting of ^{90,92,94}Zr, TPP-PEG_{24}-DFO[^{89}Zr], TPP-PEG_{24}-[FITC], TPP-PEG_{24}-DFO[^{89}Zr] and cmHsp70.1-DFO[^{89}Zr] were synthetized as described in the Supplementary Material. The *in vivo* mHsp70 targeting mAb cmHsp70.1 (21) was used as the *in vitro* gold standard for staining of mHsp70 tumor cells and for biodistribution studies. Supplementary Figure S1A–S1C provides a schematic representation of the synthesis of TPP-DFO, TPP-PEG_{24}-DFO, and TPP-PEG_{24}-[FITC].

K_d measurements by microscale thermophoresis

Binding affinities of TPP peptide tracers to Hsp70 were measured by microscale thermophoresis (MST) analysis (33, 34). For MST measurements, ^{89}Zr was replaced by a nonradioactive natural isotope (^{nat}Zr). Gradual thermophoretic changes of

Published OnlineFirst September 18, 2018; DOI: 10.1158/0008-5472.CAN-18-0707

TPP-PEG_{24}-DFO[^{nat}Zr] in a concentration range of 0.061 to 2,000 nmol/L was tested against a constant concentration of FITC-labeled recombinant Hsp70 protein (100 nmol/L; Enzo Life Sciences) in a temperature range of 20°C to 22°C using the Monolith NT (NanoTemper). The samples were incubated for 10 minutes before loading into the MST glass capillaries. As a control, a scrambled 14-mer control peptide was tested in the same molar concentration range like TPP-PEG_{24}-DFO[^{nat}Zr].

IC_{50} measurement via competition cell binding assay

The IC_{50} of the TPP-PEG_{24}-DFO[^{89}Zr] tracer was measured as reported previously (35). Briefly, 2×10^5 4T1 and CT26 cells, incubated with 30 nmol/L TPP-PEG_{24}-DFO[^{89}Zr] (18.5 kBq)/1% BSA in PBS were treated with TPP-PEG_{24}-DFO[^{nat}Zr] in a concentration range of 0 to 5,000 nmol/L at 0°C for 2 hours. After centrifugation, the pellet was washed in ice-cold PBS/1% BSA. Thereafter, the activity of the pellet and supernatant fraction was counted in a gamma-counter (Wizard Gamma Counter, Perkin-Elmer). The IC_{50} value was calculated via nonlinear regression analysis using the GraphPad Prism software (GraphPad Software).

Protein binding assay

To evaluate binding of TPP-PEG_{24}-DFO[^{89}Zr] to serum proteins, 1,110 kBq of the tracer were incubated in 500 μL of human serum for 24 hours at 37°C. Following incubation, 30 μL of the solution was eluted via size-exclusion (MicroSpin G-50 column, GE Healthcare). The activity in the eluate corresponds to bound tracer and the activity in the column corresponds to free tracer.

Cell culture

4T1 mouse mammary (ATCC CRL-2539) and CT26 mouse colon adenocarcinoma cells (CT26.WT; ATCC CRL-2638, authentication not applicable for mouse cell lines) were cultured in RPMI1640 medium supplemented with 5% FCS at 37°C under 5% CO_2 in a humidified atmosphere. The Hsp70-overexpressing tumor subline 4T1$^+$ was generated by subcloning of 4T1 tumor cells with a high mHsp70 expression. The 4T1 Hsp70$^{-/-}$ tumor cells were generated by CRISPR/Cas9-mediated knockout of the closely homologous genes *Hspa1a* and *Hspa1b*, followed by subcloning of the Hsp70$^{-/-}$ cells through limiting dilution assays, as described previously (28). Briefly, two guide sequences targeting the coding sequence (cds) of both genes were cloned into a pX462 vector and the transfected 4T1 cells were subjected to a puromycin selection. Clones were generated by limiting dilution titration and tested for knockout of Hspa1a and Hspa1b expression by Western blot analysis and flow cytometry. Cells were cultivated using 5% FCS/RPMI-based medium under standard conditions. Tumor cell lines were routinely monitored for *Mycoplasma* (MycoAlert Mycoplasma Detection Kit, Lonza), and only *Mycoplasma*-negative cells were taken for experiments. Murine primary skin fibroblasts were isolated postmortem from the dermis of Balb/c mouse following enzymatic digestion, as described in the Supplementary Material. All cell lines were used for experiments in the exponential growth phase.

Assessment of membrane Hsp70 and cellular internalization kinetics

The targeting capacity of the tested compounds and mHsp70 expression density on tumor cells and fibroblasts were assessed by flow cytometry following incubation of the FITC-labeled peptides TPP and TPP-PEG_{24} at 0°C. Flow cytometric measurement of the internalization of mHsp70-targeting probes was assessed at 37°C, as described previously (28). Briefly, after incubation of the cells for 0.5, 5, 10, 15, 30, 60, 120, and 180 minutes at 37°C, uptake was measured on a FACSCalibur instrument (BD Biosciences). Data were analyzed using CellQuest Pro software. Only propidium iodide (PI)-negative, viable cells were gated and analyzed. Internalization of the radiolabeled tracer was evaluated 10, 20, 30, 40, 50, 60, 90, and 120 minutes after incubation. Cells (4×10^6/mL) were incubated with the tracer at a working concentration of 4×10^{-8} mol/L (3×10^5 cpm/well) for one hour at 0°C. After washing, cells were resuspended in growth medium and incubated at 37°C. Then, cells were washed twice in acidic buffer (0.05 mol/L NaOAc and 0.15 mol/L NaCl at pH 2) to detach tracer that resides in the cell membrane. The final pellet was incubated with 1 mol/L NaOH (1% Triton X-100) for 3 minutes to extract the internalized pellet. The activity was measured in a gamma-counter.

Partition coefficient test

The partition coefficient of TPP-PEG_{24}-DFO[^{89}Zr] was determined by measuring the distribution of the radioactivity associated to the tracer, in equal volumes of 1-octanol and 0.01 mol/L PBS. Briefly, 0.5 MBq of the radiolabeled compound was loaded into an Eppendorf tube containing 500 μL of PBS and 500 μL of 1-octanol (Merck). After vigorous mixing for 3 minutes at room temperature, samples were centrifuged at 15,000 rpm for 1 minutes to ensure complete separation of the solvents. Then, 100-μL aliquots of each layer were withdrawn and pipetted into separate test tubes. The samples were then counted in a gamma-counter and the log *P* calculated as counts in octanol/counts in PBS solution. Four independent experiments were performed in triplicates.

Syngeneic tumor and fibroblast hyperplasia mouse models

4T1 and 4T1$^+$ mHsp70-overexpressing mammary carcinoma cells (5×10^5), CT26 colon adenocarcinoma cells (1×10^6), and 4T1 Hsp70$^{-/-}$ cells (1×10^6) were injected subcutaneously (s.c.) into the neck area of 8- to 10-week-old female Balb/c mice. To generate benign fibroblast hyperplasia viable, syngeneic primary fibroblasts (1×10^7) were implanted subcutaneously into the neck area of Balb/c mice. Tracers were injected intravenously when tumors reached a size of 0.2–0.7 cm^3, as determined by ultrasonic measurements (Logiq-5, GE Healthcare). All animal experiments were approved by the District Government of Upper Bavaria and by the District Government of Pavlov First Saint Petersburg State Medical University (St. Petersburg, Russia) and performed in accordance with the German animal welfare and ethical guidelines of the Klinikum rechts der Isar, TU Munich (Munich, Germany).

In vivo PET/CT imaging

Mice bearing mHsp70-positive 4T1 ($n = 11$), 4T1$^+$ ($n = 3$), and CT6 ($n = 8$) tumors or mHsp70-negative, benign skin fibroblast hyperplasia ($n = 3$) were anesthetized in an atmosphere of 1.5% isoflurane. 4.44 MBq of TPP-PEG_{24}-DFO[^{89}Zr] tracer was injected into the tail vein. Mice were imaged after circulation times of 1, 3, 6, 9, 16, and 24 hours, using an Inveon Docked PET/CT scanner for Small Animal (Siemens). For evaluation of the size dependency of Hsp70-targeting compounds on the biodistribution sc

Published OnlineFirst September 18, 2018; DOI: 10.1158/0008-5472.CAN-18-0707

4T1 tumor–bearing mice ($n = 5$) were injected intravenously with 2.92 MBq of cmHsp70.1-DFO[^{89}Zr], an 150-kDa anti-Hsp70 mouse IgG1 antibody, which was previously evaluated for preclinical *in vivo* tumor-targeting applications. To improve the comparability of the biodistribution of large (150 kDa; cmHsp70.1-DFO[^{89}Zr]) and small (3.5 kDa; TPP-PEG$_{24}$-DFO[^{89}Zr], circulation time: 24 hours) compounds, the falsifying effects of differently high concentrations of free tracer in the blood was minimized by choosing a circulation time of 72 hours for cmHsp70.1-DFO[^{89}Zr]. At this time-point, the blood-to-normal tissue ratio of the two compared tracers equalized. For calculation of the ratio, muscle was taken as representative of normal tissue. Anesthetized mice were positioned in the field of view (FOV) of the PET/CT scanner and underwent dynamic acquisition for 90 minutes and static PET/CT acquisition for 20 minutes. Time–activity curves of heart, liver, kidney, muscle, and tumors were generated by dynamic acquisition. Mice were monitored for breathing throughout the whole procedure and body temperature was maintained by heating pads. Images were reconstructed by 3D ordered subset expectation maximum algorithm (OSEM3D/MAP). Data are normalized and corrected for randoms, dead time, and decay with no correction for attenuation or scatter. The CT acquisition consisted of 120 projections acquired with exposure time of 200 ms, X-ray voltage of 80 kVp and anode current of 500 μA for 220° rotation. CT images were reconstructed using a modified Feldkamp algorithm.

Biodistribution analysis

After the PET/CT imaging, the animals were sacrificed and blood, tumor, and organs were taken, weighted, and counted in a gamma-counter for *ex vivo* radioactivity accumulation measurements. The results were normalized to standards. Radioactivity accumulation was calculated as percentage of the injected dose per gram of tissue (%ID/g). PET image–derived tracer uptake was quantified as %ID/g (1 cc = 1 g) in regions of interest (ROI) on the basis of CT images that were transferred to PET images. *In vivo* and *ex vivo* uptake data were compared for correlation analysis. Activity was quantified by measuring the samples for 1 minute in a gamma-counter, within an energy window of 800 to 1,000 keV for ^{89}Zr (909 keV emission).

In vivo stability analysis of TPP-PEG$_{24}$-DFO[^{89}Zr]

In vivo chemical stability of TPP-PEG$_{24}$-DFO[^{89}Zr] was evaluated in subcutaneous tumor–bearing mice at circulation times of 1, 3, 6, and 24 hours after intravenous injection of 3.0–4.0 MBq of the tracer. At each time point, mice were sacrificed and samples were taken from blood, liver, kidneys, and tumors. Urine was filtrated (Amicon Ultra, 30 kDa molecular weight cut-off, Merck KGaA). Clotted blood was centrifuged (5 minutes, 11,500 rpm), the plasma separated from the pellet, and both fractions were measured in a gamma-counter. Organs were frozen in liquid nitrogen and homogenized using a Mikro Dismembrator II ball mill (B. Braun, Melsungen, Germany). Homogenates were washed twice in 500 μL and 400 μL PBS, respectively, for 5 minutes at 11,500 rpm, supernatants of both centrifugation steps were combined, and the radioactivity of the supernatant and pellet fractions were measured separately in a gamma-counter to determine the extraction efficacy. The supernatant was filtrated (Amicon Ultra centrifugal filters), and analyzed by radio-HPLC and radio-TLC, as described in the Supplementary Material section.

Near-infrared fluorescence imaging

For fluorescence imaging experiments, Cy5.5-labeled TPP peptide and DyLight750 (DL750)-conjugated scrambled control peptide CP (OEM manufactured by Thermo Fisher Scientific) were injected intravenously in tumor-bearing mice. Twenty-four hours after administration of 100 μg of the compounds, which equals to 45 nmol/L per animal, fluorescence images were acquired by sequentially illuminating the specimens with 670 nm and 740 nm diode lasers and guiding the emitted fluorescence through appropriate emission filters. For capturing of the signals, a back illuminated EM-CCD camera (iXon DU888) was used. The fluorescence-imaging procedure was described previously in more detail (29).

Histology and light sheet ultramicroscopy

IHC stainings of Hsp70, CD31-positive vascular endothelial cells, F4/80-positive murine macrophages were performed as described previously (21). Briefly, 5-μm tissue sections were obtained from tumors used for PET imaging and biodistribution studies. Antigen retrieval (pH 6) was followed by incubation with primary antibodies and consecutively with horseradish peroxidase–conjugated secondary mAb (DAKO, Agilent) and visualized with 3,3′-diamino-benzidine. IHC of Ki67 (Abcam)-positive, proliferating cells has been performed accordingly. Macrophages and vessels were quantified at representative ROI of three different tumor sections and normalized to mm^2. Standard hematoxylin and eosin (H&E) staining was used for conventional morphologic evaluation. To evaluate the vascular density throughout the whole tumor, ultramicroscopic analysis of cleared tissues was performed after injection of AlexaFluor 750–labeled lectin (Lectin-AF750). Briefly, 1 μmol/L of Lectin-AF750 was injected intravenously, 15 minutes prior sacrificing. Excised tissue was fixated in Paxgene Tissue Fix (PreAnalytix), cleared following the iDISCO method (36) and imaged by light sheet ultramicroscopy (LaVision Biotec).

Statistical analysis

Statistical analysis was performed using Student *t* test for unpaired data. Two-sided significance levels of the comparison between two groups were calculated and ***, $P < 0.001$; **, $P < 0.01$ and *, $P < 0.05$ values were considered as statistically significant.

Results

Molecular characterization of TPP derivatives and cmHsp70.1-DFO[^{89}Zr]

The tumor cell–penetrating peptide (TPP) comprises the amino acid sequence aa$_{450–463}$ (TKDNNLLGRFELSG; TPP) of the C-terminal localized oligomerization domain of Hsp70 that is exposed on the plasma membrane of tumor cells. Herein, the novel radiolabeled tumor-specific TPP-PEG$_{24}$-DFO[^{89}Zr] PET tracer, consisting of the TPP peptide sequence for tumor cell–specific binding, a PEG$_{24}$ moiety for stability and a DFO-activated reporter system, was firstly applied for *in vivo* tumor imaging in different preclinical models. Tumor specificity was validated using a custom-made FITC-labeled version of the tracer (TPP-[FITC], EMC microcollections; Fig. 1A; ref. 29). The intermediate products of the synthesis of TPP-PEG$_{24}$-DFO[^{89}Zr] were controlled for quality. The insertion of a cysteine residue at the N terminus of TPP ([C]TKDNNLLGRFELSG-acid) enabled maleimide conjugation. The TPP-DFO derivative was synthesized at a high yield of 84% by a reaction of DFO-maleimide with the thiol group of the

Published OnlineFirst September 18, 2018; DOI: 10.1158/0008-5472.CAN-18-0707

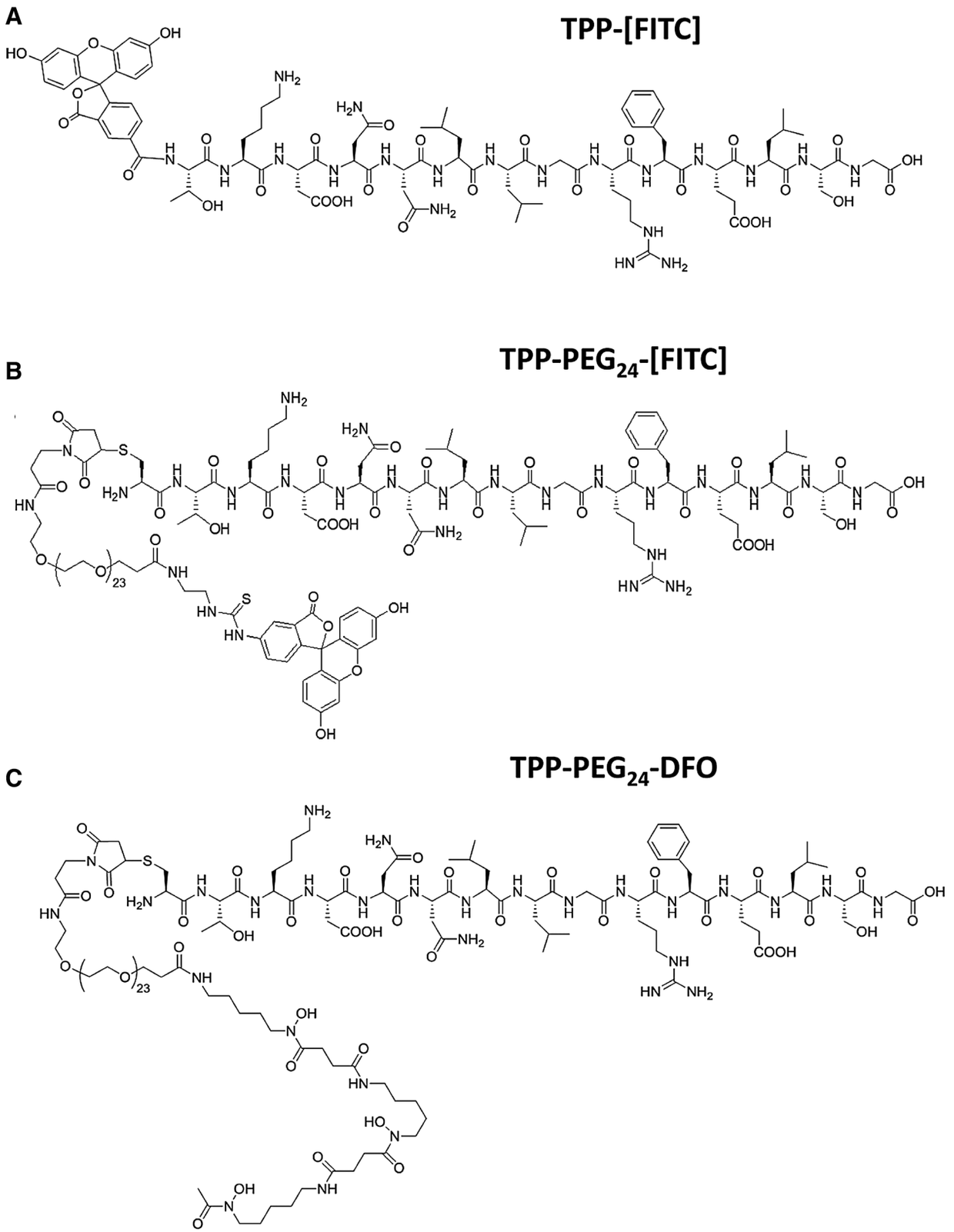

Figure 1.
Chemical structures and molecular weights of TPP-[FITC] (1,975 g/mol; **A**), TPP-PEG_{24}-[FITC] (3,396 g/mol; **B**), and TPP-PEG_{24}-DFO (3,505 g/mol; **C**).

Published OnlineFirst September 18, 2018; DOI: 10.1158/0008-5472.CAN-18-0707

terminal cysteine in DMSO/PBS (~1:10) and the final product was purified by semi-preparative HPLC-MS (Supplementary Experimental Material; Supplementary Fig. S2A). Because the sequence of TPP is part of the oligomerization domain of Hsp70, the peptide has the tendency to form self-aggregates, which can be reduced by insertion of a heterobifunctional PEG_{24} moiety to the maleimide and N-hydroxysuccinimide–activated ester groups (mal-PEG_{24}-NHS), as a spacer between peptide and imaging reporter molecule (FITC or DFO chelator). Therefore, mal-PEG_{24}-NHS was firstly reacted to FITC-NH_2 (37) or DFO and then, the resulting conjugates were reacted with the TPP peptide moiety utilizing the maleimide-thiol Michael addition reaction (Supplementary Fig. S1B and S1C). High yields of the products TPP-PEG_{24}-[FITC] (Fig. 1B) and TPP-PEG_{24}-DFO (Fig. 1C) were obtained after purification by semi-preparative HPLC-MS and ESI mass spectrometry (Supplementary Fig. S2A–S2F). Finally, TPP-PEG_{24}-DFO[^{89}Zr] and TPP-PEG_{24}-DFO[^{nat}Zr] were prepared by adding ^{89}Zr-oxalate and ^{nat}Zr-oxalate, respectively, to an aqueous solution of the peptide at pH6.5. ^{89}Zr was used as a reporter isotope because of the long circulation time of the peptide complex. Characterization, radio-HPLC analysis and stability testing of the radiolabeled tracers (TPP-peptide, cmHsp70.1 mAb) are described in the Supplementary Material and Supplementary Fig. S3A–S3D.

Specific binding and uptake of TPP-based tracers reflect mHsp70 expression patterns of tumor cells and primary fibroblasts *in vitro*

Cytosolic Hsp70 expression in the different tumor cell lines 4T1, 4T1$^+$, and CT26 and primary mouse skin fibroblasts was determined by an Hsp70 ELISA using identical instrument settings and image processing (Fig. 2A). The Hsp70 overexpressing, highly metastatic mouse mammary carcinoma cell line 4T1$^+$ showed significantly higher cytosolic Hsp70 levels (mean fluorescence intensity 138,517 ± 14,839 au), than wild-type 4T1 (mean 118,280 ± 9015 au; $P < 0.05$), and mouse adenocolon carcinoma cell line CT26 (mean 92,170 ± 9,235 au; $P < 0.01$). The cytosolic Hsp70 content of primary skin fibroblasts was significantly lower than that of all tumor cells ($P < 0.001$) with a mean signal intensity of only 8,019 ± 5,177 au. The specific binding of TPP-PEG_{24}-[FITC] to mHsp70 on viable tumor (4T1, 4T1$^+$, CT26) and normal (fibroblasts) cells was compared with that of the previously established fluorescence-labeled cmHsp70.1-[FITC] mAb and TPP-[FITC] peptide (Fig. 2B and C; refs. 21, 29). Following suppression of the metabolic activity at 0°C, FITC-labeled cmHsp70.1 mAb, TPP peptide and TPP-PEG_{24} showed comparable binding pattern with 4T1 (82%, 66%, 64%, respectively), 4T1$^+$ (97%, 99%, 100%, respectively), and CT26 (68%, 54%, 59%, respectively) tumor cells and single-cell suspensions of primary mHsp70-negative skin fibroblasts (5%, 1%, 3%, respectively; Fig. 2B). A histogram overlay following TPP-PEG_{24}-[FITC] and TPP-[FITC] staining of 4T1 tumor cells revealed comparable binding patterns and mean fluorescence intensity values (MFI; 33.5 ± 111 au, 23.1 ± 66 au, respectively; Fig. 2C).

The internalization kinetics of mHsp70-specific peptide tracers was evaluated by incubation under physiologic conditions (37°C, 5% CO_2). FACS analysis after 0.5, 5, 10, 15, 30, 60, 120, and 180 minutes revealed a rapid and comparable internalization of the 2.0 kDa TPP-[FITC] and 3.5 kDa TPP-PEG_{24}-[FITC] in both tumor cell types 4T1 and CT26 (Fig. 3A). After 30 minutes, MFI values increased 5.6-fold and 7.3-fold after incubation of 4T1 cells with TPP-[FITC] and TPP-PEG_{24}-[FITC], respectively. The increase was calculated as the quotient of the MFI value at 37°C (30 minutes) to the MFI value at 0°C (30 minutes). Under identical conditions, CT26 cells showed a 9.7-fold (TPP-[FITC]) and 6.7-fold (TPP-PEG_{24}-[FITC]) intracellular increase in MFI with the respective probes. A dotted staining pattern, which is typical for an endolysosomal internalization pathway, was apparent after a 30-minute incubation period with both compounds in 4T1, 4T1$^+$, and CT26 tumor cells (Fig. 3B).

4T1 and CT26 tumors show comparable macrophage infiltration and microvessel density, but different Hsp70 expression

Apart from chemical features of the tracer, the intratumoral accumulation *in vivo* can be influenced by the architecture of tumor vessels and the tumor microenvironment including phagocyting macrophages. Therefore, the Hsp70 content was analyzed concomitantly with tumor-associated macrophages and the tumor vasculature in sections of 4T1 and CT26 tumors. In line with results obtained from *in vitro*–cultured tumor cells, the cytosolic Hsp70 content was higher in 4T1 compared with CT26 tumors (Fig. 4A). Both tumor models revealed a high nuclear Hsp70 staining intensity. A representative view of a histologic section of a subcutaneous benign fibroblast hyperplasia with a central necrosis (N; Supplementary Fig. S4A) shows a very weak Hsp70 staining intensity in the viable part of the tissue (Supplementary Fig. S4B and S4C).

Tumor-infiltrating macrophages as visualized by F4/80 antibody staining showed comparable numbers in both tumor mouse models (4T1: 1,214 ± 247 cells/mm^2 and CT26: 1,187 ± 222 cells/mm^2; Fig. 4B). Previous work indicated that macrophages do not display Hsp70 on their plasma membrane (29).

The main supply route for delivery of intravenously injected compounds is the tumor vasculature. To exclude a bias induced by a divergent vascularization, a lectin-based light sheet ultramicroscopy of excised tumors was performed concomitantly with a staining of endothelial cells in tumor sections using CD31 mAb. As shown in Fig. 4C, a high vessel density was detectable in viable tumor regions of both mouse models. However, the vascular architecture differed in 4T1 and CT26 tumors. 4T1 tumors showed a distribution of relatively large vessels throughout the whole viable tumor mass, whereas in CT26 tumors, the fraction of main feeding vessels was lower in the central tumor area. In contrast, the distribution of microvessels was comparably high in viable tumor areas of both tumor models. In line with the results of light sheet microscopy, a CD31 staining of representative tumor areas of both models revealed a comparable, homogeneous distribution of capillaries with less than 1,500 μm^2 of lumen. As shown in Fig. 4D, the microvessel density was 110 ± 25 (4T1) and 120 ± 43 capillaries (CT26) per mm^2 tumor tissue. No significant differences were observed in 4T1 and 4T1$^+$ tumors (4T1: 110 ± 25; 4T1$^+$: 105 ± 11). In summary, tumors differ only in their Hsp70 content (Figs. 2 and 4A), but not with respect to the number of tumor-infiltrating macrophages or microvessel density.

Accumulation of TPP-PEG_{24}-DFO[^{89}Zr] in tumor mouse models reflects mHsp70 expression of the tumor cells

The K_d of TPP-PEG_{24}-DFO[^{nat}Zr] was determined as 18.9 ± 11 nmol/L by MST measurements (Supplementary Fig. S5A) and the IC_{50} (38 ± 2) and log *P* value of the compound (−3.60 ± 0.2)

Published OnlineFirst September 18, 2018; DOI: 10.1158/0008-5472.CAN-18-0707

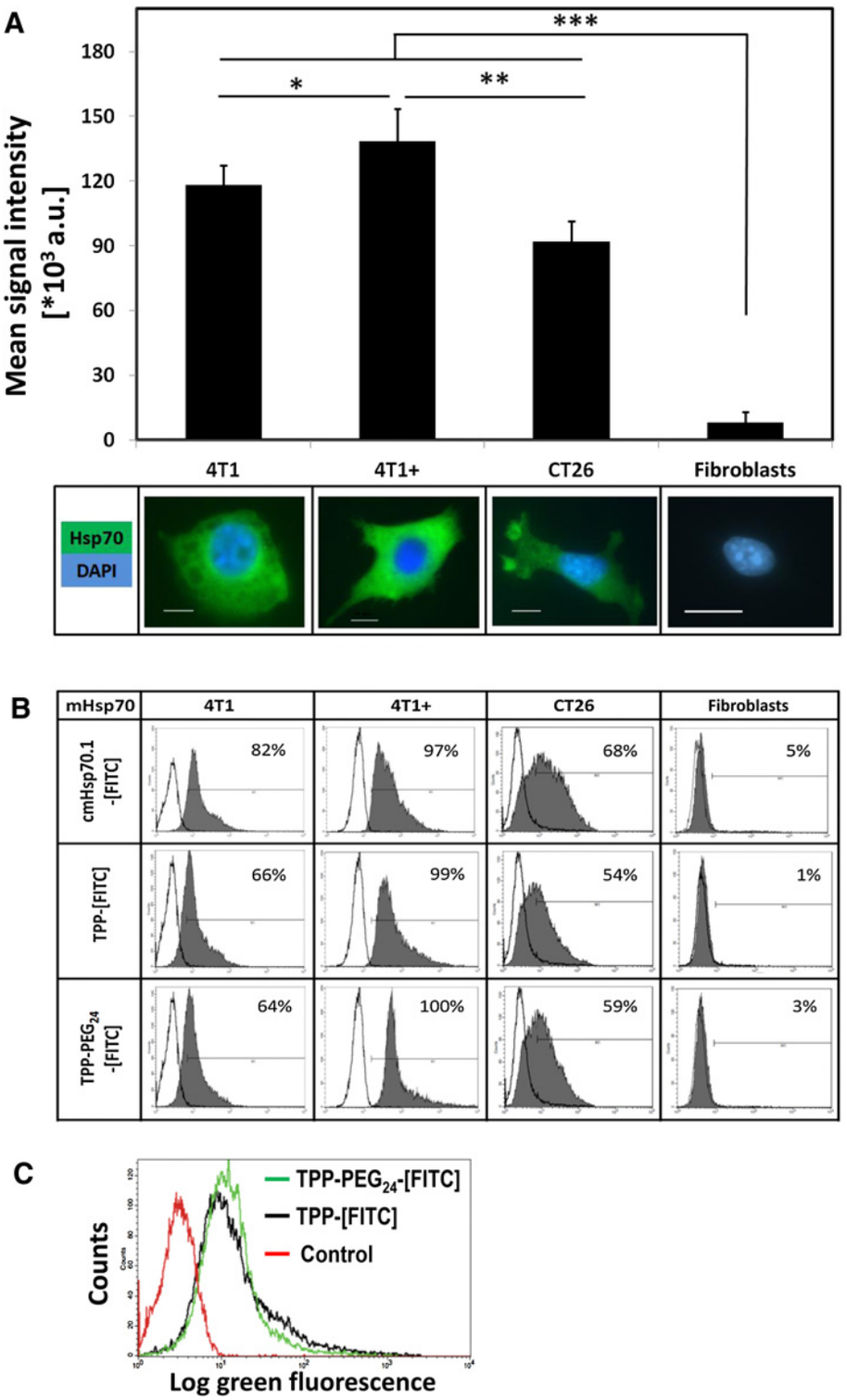

Figure 2.
Comparative analysis of *in vitro* Hsp70 expression of 4T1, 4T1^{+}, CT26 tumor cell lines, and subcutaneous fibroblast hyperplasia (fibroblasts). **A,** Top, mean signal intensity of cytoplasmic staining, as determined by in-cell ELISA based quantification. Bottom, representative immunfluorescence images of the cells following intracellular Hsp70 staining, using cmHsp70.1 mAb. Blue, DAPI; green, cmHsp70.1-[FITC]. Scale bar, 5 μm. **B,** Comparative analysis of *in vitro* expression profiles of membrane-bound Hsp70 on 4T1, 4T1^{+}, CT26 tumor cell lines, and subcutaneous fibroblast hyperplasia (fibroblasts) using cmHsp70.1-[FITC] mAb (top), TPP-[FITC] peptide (middle), and TPP-PEG$_{24}$-[FITC] peptide (bottom). **B,** Flow cytometry profiles of mHsp70 staining patterns after incubation of the probes at 0°C. Percentages of positively stained, viable cells are indicated in each histogram. **C,** Overlay of flow cytometric histograms of 4T1 cells stained with TPP-[FITC] (black line) and TPP-PEG$_{24}$-[FITC] (green line). Red line, histogram of an isotype-matched control antibody.

are shown in Supplementary Fig. S5B. The internalization kinetics of the newly developed TPP-based PET tracer in 4T1 cells over a period of 240 minutes is shown in Supplementary Fig. S5C.

The *in vivo* specificity and target enrichment capacity of the tracer was studied in four preclinical models with different mHsp70 expression patterns. TPP-PEG$_{24}$-DFO[^{89}Zr] was evaluated by micro-PET/CT acquisition in mHsp70-positive 4T1, 4T1^{+}, CT26 tumor mouse models and mHsp70-negative benign fibroblast hyperplasia. From PET measurements (1–24 hours; Fig. 5A), a short-term (Supplementary Fig. S5D) and long-term

Published OnlineFirst September 18, 2018; DOI: 10.1158/0008-5472.CAN-18-0707

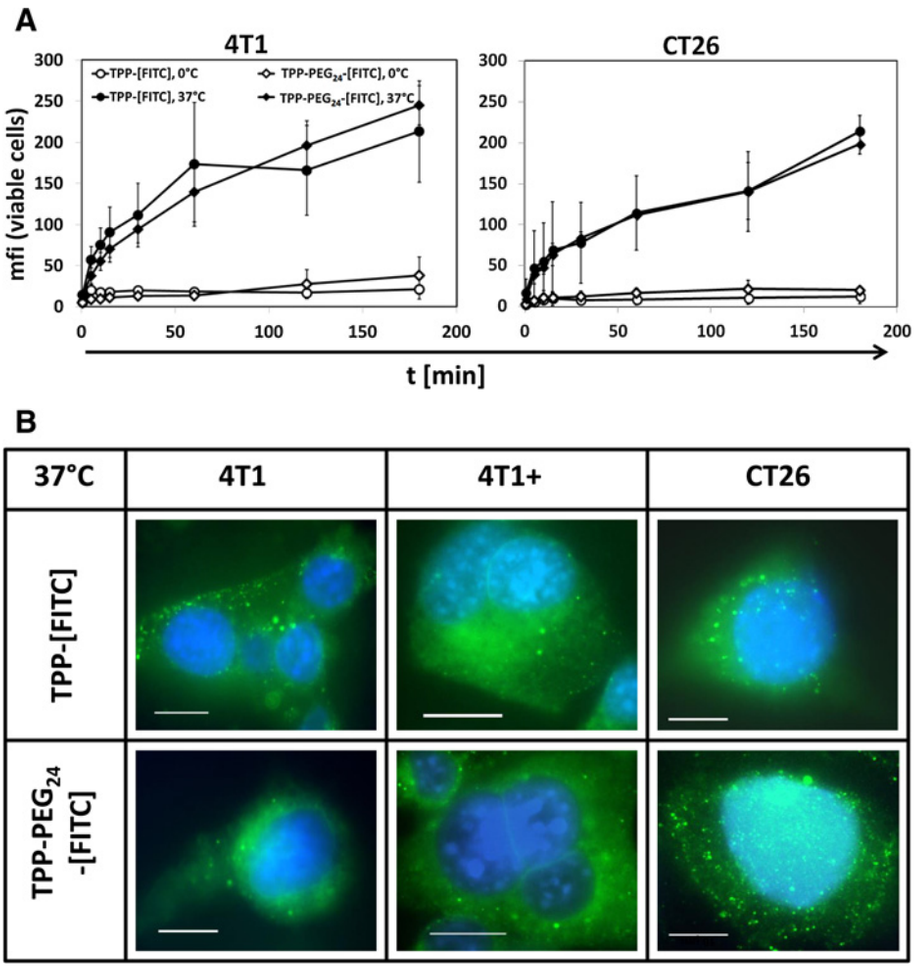

Figure 3.

In vitro dynamics of uptake of mHsp70-targeting probes into viable tumor cells at 0°C and 37°C. **A,** Kinetics of the binding and uptake of TPP-[FITC] (circles) and TPP-PEG_{24}-[FITC] (diamonds) into 4T1 (left graph) and CT26 (right graph) tumor cells at 0°C (open symbols) and 37°C (filled symbols) as determined by mean arbitrary units (au) of fluorescence intensity (mfi) signals. Data show the mean of two to three independent experiments ± SD. **B,** Representative immunofluorescence images of 4T1, $4T1^{+}$, CT26 tumor cells, following incubation with TPP-[FITC] (top) and TPP-PEG_{24}-[FITC] (bottom) peptide-based compounds at 37°C for 30 minutes. Scale bar, 10 μm.

(Supplementary Fig. S5E) time–activity analysis was performed by defining volumes of interest on selected organ scans (4T1 tumor, CT26 tumor, heart, liver, muscle). Tumors could be firstly distinguished from normal tissues 3 hours postinjection, when TPP-PEG_{24}-DFO[^{89}Zr] tracer was still visible in the blood stream (heart signal). Six hours after tracer injection, the tumors were clearly distinguishable from surrounding tissues and the background activity in heart and liver dropped continuously until 24 hours (Supplementary Fig. S5E). Image-derived uptake calculations, based on median uptake values obtained by static scans (5 mice), revealed a maximum accumulation of TPP-PEG_{24}-DFO[^{89}Zr] and highest tumor-to-background contrast, 24 hours after tracer injection in 4T1 (2.66 ± 0.50%ID/g) and CT26 (2.00 ± 0.4%ID/g) tumors. This signal increase in the tumor was accompanied by a drastic decrease of the tracer in the blood pool (Supplementary Fig. S5E). The kinetics of target accumulation of TPP-PEG_{24}-DFO[^{89}Zr] tracer was comparable in $4T1^{+}$ and 4T1 tumors (Supplementary Fig. S5E).

Uptake of the tracer in the gall bladder after static acquisition was observed only at early time points (1–3 hours), which is indicative for a partial excretion via the hepatobiliary pathway (Fig. 5A). Specificity and sensitivity of the TPP-based tracer for mHsp70 expression density on tumor cells was demonstrated in mice bearing 4T1 tumors (left neck) and CT26 tumors (right neck; Fig. 5A) or benign mouse skin hyperplasia (Fig. 5B), which do not show mHsp70 expression. The highest uptake of TPP-PEG_{24}-DFO[^{89}Zr] tracer was detected 24 hours after intravenous injection in 4T1 tumors followed by CT26 tumors. In contrast, 24 hours after tracer injection, the uptake was comparable to that of background in benign skin hyperplasia (Fig. 5B). Prominent residual activity was present in the kidneys and bladder due to the renal excretion of the peptide-based tracer. For further evaluation of the *in vivo* specificity of TPP to membrane-Hsp70 on tumor cells, near-infrared imaging on tumor-bearing mice harboring both, subcutaneous 4T1 wt and subcutaneous 4T1 $Hsp70^{-/-}$ tumors, was performed. Thereby, 4T1 $Hsp70^{-/-}$ cells served as a negative control. Mice were simultaneously injected with TPP[Cy5.5] and the scrambled control peptide CP[DL750]. Twenty-four hours after intravenous injection, animals were sacrificed and imaged for fluorescence. The signal ratios of tumors and tumor-surrounding normal tissues (tumor-to-background ratios, TBR) were calculated and used as a surrogate marker for tumor-specific accumulation of the tracers.

In epifluorescence experiments, TBR of TPP-[Cy5.5] in 4T1 Hsp70 wt tumors was significantly higher, compared with that of CP-[DL750] in 4T1 wt tumors, or to that of both compounds in 4T1 $Hsp70^{-/-}$ tumors (Supplementary Fig. S6A). Following tumor dissection, accumulated tumor signals of the two

Published OnlineFirst September 18, 2018; DOI: 10.1158/0008-5472.CAN-18-0707

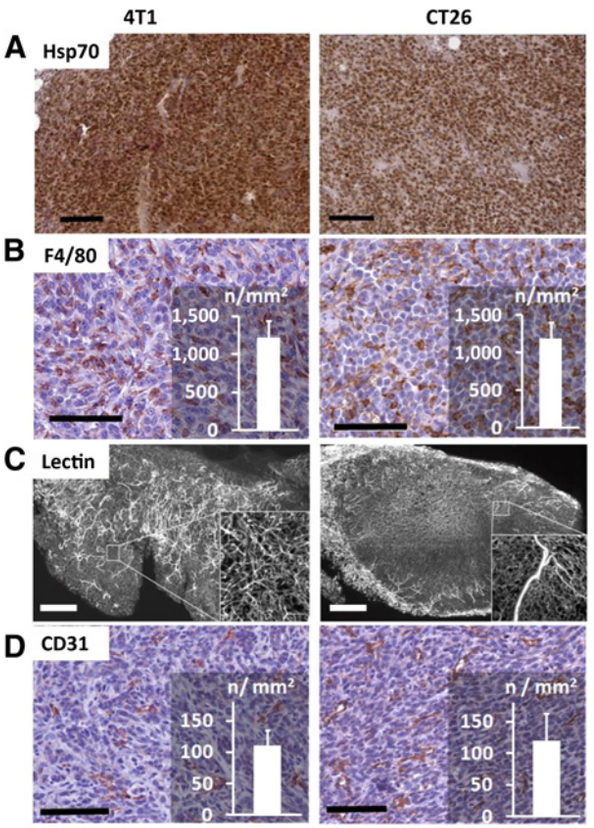

Figure 4.

Representative FFPE sections of subcutaneously grown tumors stained for Hsp70, F4/80-positive tumor-infiltrating macrophages, and CD31-positive blood vessels. **A,** IHC staining of Hsp70 on FFPE sections of 4T1 (left) and CT26 (right) using cmHsp70.1 mAb. Scale bar, 200 μm. **B,** IHC staining of tumor-infiltrating macrophages on FFPE sections of 4T1 (left) and CT26 (right) tumors using F4/80 mAb. Scale bar, 100 μm. The number of F4/80-positive cells (n) per $mm^2 \pm$ SD are indicated in the white inset bar graph. **C,** Representative light sheet microscopical views of 4T1 (left) and CT26 (right) tumors, 15 minutes after intravenous injection of 250 μg of Lectin-[AF750] (white signals). Scale bar, 1 mm. **D,** IHC staining of the tumor vasculature on FFPE sections (5 μm) of 4T1 (left) and CT26 (right) using CD31 mAb. Scale bar, 100 μm. The number of CD31-positive cells (n) per $mm^2 \pm$ SD are indicated in the white inset bar graph.

compounds in wt and Hsp70$^{-/-}$ 4T1 tumors were compared. Gray intensity values of the images were plotted along a horizontal line through the tumors of one mouse. The peak signal intensity of TPP[Cy5.5] in a 4T1 wt tumor was twice as high, compared with that in a Hsp70$^{-/-}$ tumor. These data further demonstrate the Hsp70 specificity of the TPP peptide, *in vivo*. A scrambled control peptide CP[DL750] revealed a similar low background signal in both tumors, Hsp70 wt and 4T1 Hsp70$^{-/-}$ tumors (Supplementary Fig. S6B).

Biodistribution studies

Biodistribution studies were performed in 6- to 8-week-old, female mice with 4T1 (left neck), and CT26 (right neck) or 4T1^{+} (right neck) tumors. All mice underwent PET/CT imaging 24 hours post intravenous injection of TPP-PEG_{24}-DFO[^{89}Zr]. After washing, excised tumors and organs were weighted and counted in a gamma-counter. The calculated tracer uptake in 4T1^{+}, 4T1 and CT26 tumors was 6.2 ± 1.1, 4.3 ± 0.7 and 3.39 ± 0.77%ID/g, respectively, and 0.24 ± 0.03%ID/g in benign fibroblast hyperplasia, which served as a negative control (Fig. 6A). The intratumoral distribution of TPP-PEG_{24}-DFO[^{89}Zr], as determined by PET/CT, showed a ring-shaped staining pattern within the viable rim area of the tumor (Fig. 6B). No PET signal was detectable in the central necrotic tumor area, which was confirmed by H&E staining (Fig. 6C), IHC for the proliferation marker Ki67 and for the endothelial cell marker CD31. Both stainings were only detectable in viable, but not in necrotic tumor tissue (Fig. 6D and E). This finding shows that the tracer accumulates selectively in viable tumor tissue. The uptake of TPP-PEG_{24}-DFO[^{89}Zr] in 4T1^{+}, 4T1 and CT26 tumors and fibroblasts differed significantly ($P < 0.01$; Fig. 6F). Because of the size and hydrophilicity of the tracer, uptake in the liver was low (0.32 ± 0.14%ID/g) and in kidney high (26.21 ± 4.38%ID/g). In all tumors, independently of their origin, a correlation between PET derived *in vivo* and *ex vivo* tracer enrichment measurements could be confirmed ($R^2 = 0.847$; Fig. 6G).

For evaluation of the dependency of biodistribution on the tracer size, the full-length murine IgG1 antibody-based PET-tracer cmHsp70.1-DFO[^{89}Zr] ($K_D = 5.4$ nmol/L) was compared to the 3.5 kDa TPP-PEG_{24}-DFO[^{89}Zr] ($K_D = 18.9$ nmol/L). As expected, the 150 kDa cmHsp70.1-DFO[^{89}Zr] showed the typical long blood half-life and liver enrichment of IgG antibodies. For a better comparability of the two compounds, a circulation time of 72 h was taken for cmHsp70.1-DFO[^{89}Zr], and compared with 24 hours for TPP-PEG_{24}-DFO[^{89}Zr], after intravenous injection. The different circulation times were chosen to minimize falsifying effects on organ contents, which can be induced by different tracer concentrations remaining in the vascular system of the respective organs. At the indicated time points, TPP-PEG_{24}-DFO[^{89}Zr] and cmHsp70.1-DFO[^{89}Zr] displayed comparable blood-to-muscle signal ratios of 6.4 ± 0.2 and 6.6 ± 1.4, respectively. These equal ratios are indicative for a comparable extravasation status of both compounds. In PET studies on 5 mice, cmHsp70.1-DFO[^{89}Zr] revealed the typical biodistribution pattern of a 150 kDa, full-length IgG1 antibody, characterized by a high liver uptake and a long blood half-life. A direct comparison of the antibody- and the peptide-based tracer showed significantly higher accumulation ($P < 0.05$) of DFO[^{89}Zr]-labeled cmHsp70.1 tracer in the main healthy organs, such as spleen, pancreas, lung, duodenum, heart, bone and muscle, compared with the 3.5 kDa TPP-PEG24-DFO[^{89}Zr] (Fig. 7). Although the enrichment of cmHsp70.1-DFO[^{89}Zr] in sc 4T1 wt tumors was higher, compared with TPP-PEG_{24}-DFO[^{89}Zr] (13.4 ± 2.1%ID/g and 4.3 ± 0.7%ID/g, respectively), the TPP-peptide based compound showed favorable tumor-to-normal organ ratios due to the minimal residual signal in most normal organs. As an example, *in vivo* application of TPP-PEG_{24}-DFO[^{89}Zr] displayed a tumor to muscle ratio of 33.0 ± 1.1, compared with a tumor-to muscle ratio of 10.3 ± 2.0, as determined by biodistribution of cmHsp70.1-DFO[^{89}Zr].

In vivo stability analysis of TPP-PEG24-DFO-[^{89}Zr]

For *in vivo* stability analysis, mice were injected with 3.0–4.0 MBq of TPP-PEG_{24}-DFO[^{89}Zr] and sacrificed 1, 3, 6, and 24 hours postinjection. Autoradiographs of TLC loaded with homogenized samples of blood, kidney, liver, 4T1, and CT26 tumors, showed that up to 24 hours after intravenous administration, intact TPP-PEG_{24}-DFO[^{89}Zr] was present in all tested organs

Published OnlineFirst September 18, 2018; DOI: 10.1158/0008-5472.CAN-18-0707

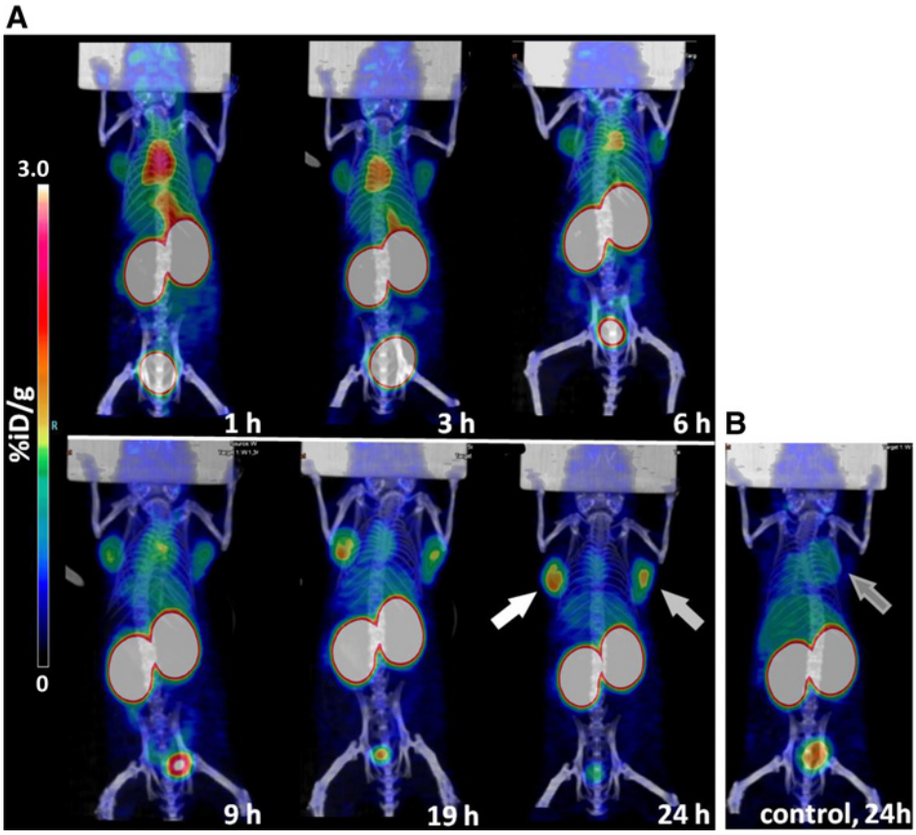

Figure 5.
Representative PET scans of viable, tumor-bearing mice, following the kinetics of tracer biodistribution within the first 24 hours after intravenous injection of TPP-PEG_{24}-DFO[^{89}Zr]. **A,** Pseudocolor images of static PET scans of a mouse bearing 4T1 (left, white arrow) and CT26 (right, gray arrow) tumors, scanned at circulation times of 1, 3, 6, 9, 19, and 24 hours. **B,** Representative PET scan of a mouse bearing mHsp70-negative, subcutaneously implanted, benign fibroblast hyperplasia as a control (dark gray arrow) after a circulation time of the compound of 24 hours.

(Supplementary Fig. S7A). This result was confirmed by radio-HPLC showing a single peak with a retention time at 16.50 minutes, corresponding to the TPP-PEG_{24}-DFO-[^{89}Zr] in blood and kidney (Supplementary Fig. S7B).

Discussion

Research on the development of clinically applicable, tumor-specific tracers with potential prognostic relevance remains indispensable (38–40). The membrane-bound form of the major stress-inducible 72-kDa Hsp70 is exclusively found on the plasma membrane of viable tumor cells of multiple entities (3, 4, 15), and therefore qualifies as a universal tumor-specific target for imaging. Preclinical therapeutic approaches using the mHsp70-specific cmHsp70.1 mAb for targeting mHsp70 on tumor cells revealed an ample tumor-specific binding and intratumoral accumulation *in vivo* that results in a significant activation of the host's antibody-dependent cellular antitumor immune response (21). Because of the size, biodistribution characteristics and immunogenicity, full-length antibodies exhibit certain limitations for diagnostic purposes (22, 41). In comparison, smaller molecules such as peptides display certain beneficial features over antibodies for *in vivo* applications, including short circulation periods, fast body clearance, favorable biodistribution, improved ingress into solid tumors and highly efficient tumor cell penetration capabilities (26, 42–44). Consequently, we developed the Hsp70-specific 14-mer peptide tracer based on TPP that enables tumor cell specificity by mimicking the characteristics of the Hsp70 oligomerization domain. *In vivo* validation of a fluorescence-labeled TPP derivative in syngeneic and xenograft human tumor mouse models of 6 different entities exhibited universal tumor enrichment capacity and notable tumor cell specificity (29). In contrast, cells of the tumor microenvironment were found to be mHsp70-negative. The clinical relevance for an Hsp70-based tumor targeting is further given by a correlation of a high Hsp70 expression with inferior patient survival and therapy resistance in multiple tumor entities, such as carcinomas of the gastrointestinal tract (20), squamous cell carcinoma of the head and neck (12), esophageal carcinoma (16), or prostate carcinoma (11). Therefore, *in vivo* targeting of mHsp70 with TPP-PEG_{24}-DFO[^{89}Zr] offers, apart from its tumor-specific targeting capacity, also the potential to predict clinical outcome or therapy responses. The significantly enhanced accumulation of TPP-PEG_{24}-DFO[^{89}Zr] in highly malignant, metastasizing 4T1 mammary carcinomas compared with the lower malignant CT26 colon carcinomas also supports this finding. Another beneficial feature of the mHsp70-based *in vivo* tumor imaging is the high turnover-rate of mHsp70 into the cytosol of tumor cells via an alternative endolysosomal pathway, which enables the intracellular accumulation of intravenously injected Hsp70-targeting tracers. As a result an enhanced TBR is achieved by an extension of the time period for wash-out of unspecific tracer binding to normal tissues. In previous studies, near-infrared optical imaging showed superior TBR in subcutaneously implanted and endogenous tumor mouse models, following intravenous administration, compared with a unspecific control peptide probe (29). In comparison with an $a_v ß_3$ integrin–targeting small-molecule tracer, TPP peptide–based probes revealed higher tumor-specific enrichment, because

Published OnlineFirst September 18, 2018; DOI: 10.1158/0008-5472.CAN-18-0707

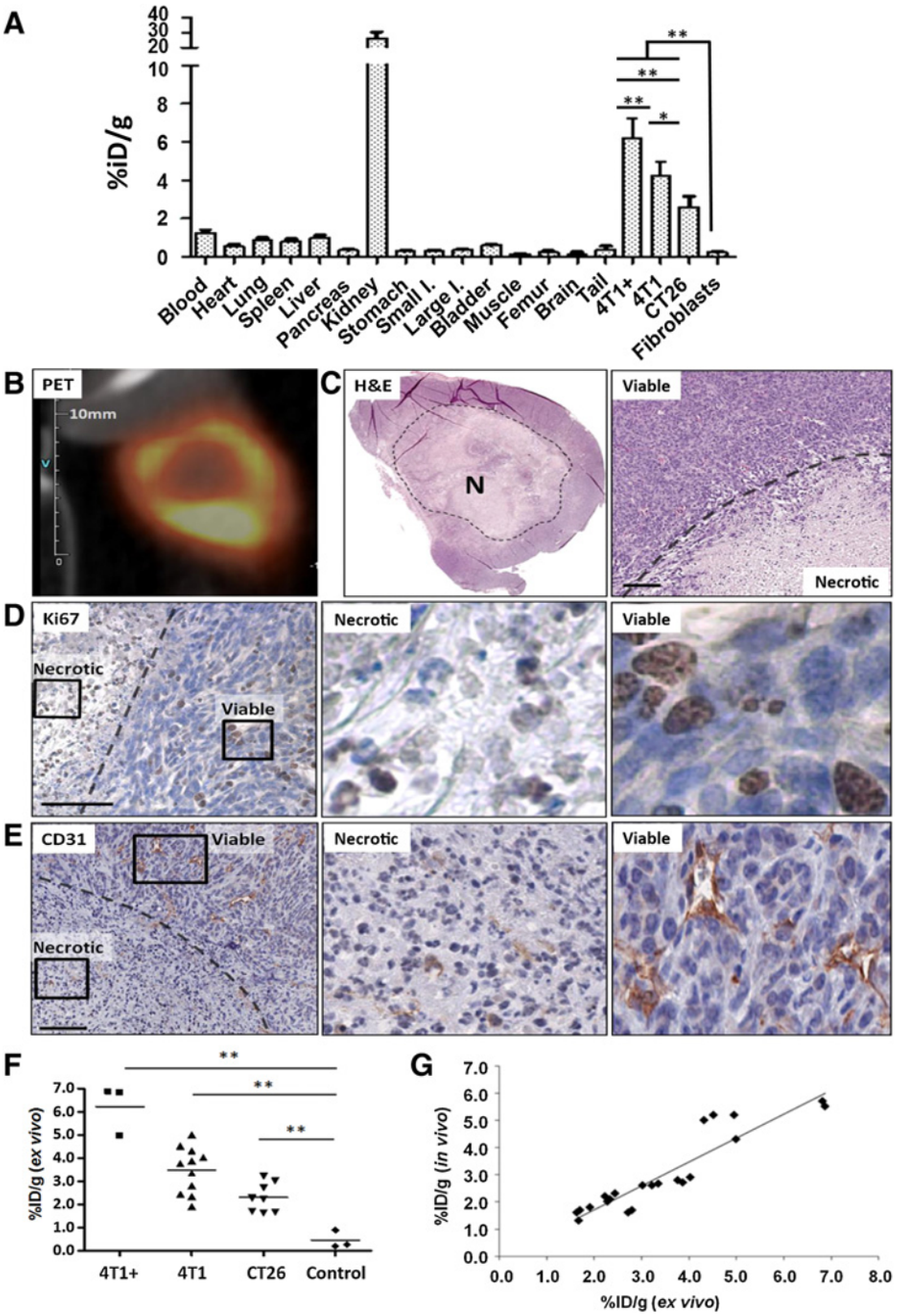

Figure 6.

Biodistribution study 24 hours after intravenous injection of TPP-PEG_{24}-DFO[^{89}Zr] in mHsp70-positive 4T1 ($n = 11$), 4T1^{+} ($n = 3$), and CT26 ($n = 8$) tumor-bearing as well as mHsp70-negative, benign hyperplasia-bearing ± mice ($n = 3$). **A,** Quantification of the tracer accumulation in organs and tumors of the mice, given in mean values ± SD. **B,** Intratumoral, ring-shaped accumulation of the PET tracer TPP-PEG_{24}-DFO[^{89}Zr] in viable tumor tissue, but not in the central necrotic area of 4T1 tumor. **C,** Representative H&E staining of the ring-shaped, viable 4T1 tumor with a large central necrosis at two magnifications. **D,** Ki67 staining of proliferative tumor cells in the viable tissue (right), but not in the central necrosis (left). Magnified excerpts of the staining within necrotic and viable tissue areas, as indicated by the rectangular insets, are shown on the right. Scale bar, 100 μm. **E,** CD31 staining of a tumor area containing viable tumor tissue (top right) and central necrosis (bottom left). Magnified excerpts of the staining within necrotic and viable tissue areas, as indicated by the rectangular insets, are shown on the right. Vascularization is visible in the viable tumor tissue, but not in the central necrosis. Scale bar, 100 μm. **F,** Comparative analysis of the tracer accumulation derived from all mHsp70-positive tumor and mHsp70-negative benign fibroblast hyperplasia mouse models. The tracer accumulation in the different models differed statistically significant (**, $P < 0.01$). **G,** PET-image based determination of *in vivo* tracer uptake versus organ-derived uptake calculation (*ex vivo*). Uptake is given in %ID/g, correlation coefficient ($R^2 = 0.874$).

$a_v ß_3$ integrin is also expressed on nonmalignant cells such as tumor-associated macrophages and tumor-infiltrating fibroblasts. Intratumoral uptake of the fluorescence-labeled TPP probe was confirmed by histologic analysis of cryopreserved tumors after intravenous injection of the probe. Therefore, the TPP-based fluorescence probe was developed into a PET tracer after radiolabeling using the ^{89}Zr-DFO methodology. The *in vivo* epifluorescence imaging technique was used to confirm Hsp70 specificity of the peptide-based compound after intravenous injection into mice bearing subcutaneous Hsp70 wt and Hsp70$^{-/-}$ 4T1 tumors. Fluorescence-labeled TPP peptide specifically accumulated in Hsp70 wt but not in Hsp70$^{-/-}$ tumors. Because TPP is part of the oligomerization domain of Hsp70, the peptide has the tendency to self-aggregate in solution, which adversely affects its *in vivo* distribution. Therefore, an optimized PEGylated ^{89}Zr-radiotracer (TPP-PEG_{24}-DFO[^{89}Zr]) was developed. *In vitro* characterization of FITC-labeled TPP-PEG_{24} conjugates showed a comparable capacity to bind mHsp70 on different tumor cell lines like full-length cmHsp70.1 mAb. The long *in vivo* circulation time of the tracer enables optimal accumulation and high tumor-to-background ratios 24 h after tracer injection. Furthermore, internalization of the PET tracer into mHsp70-positive tumor cells was

Published OnlineFirst September 18, 2018; DOI: 10.1158/0008-5472.CAN-18-0707

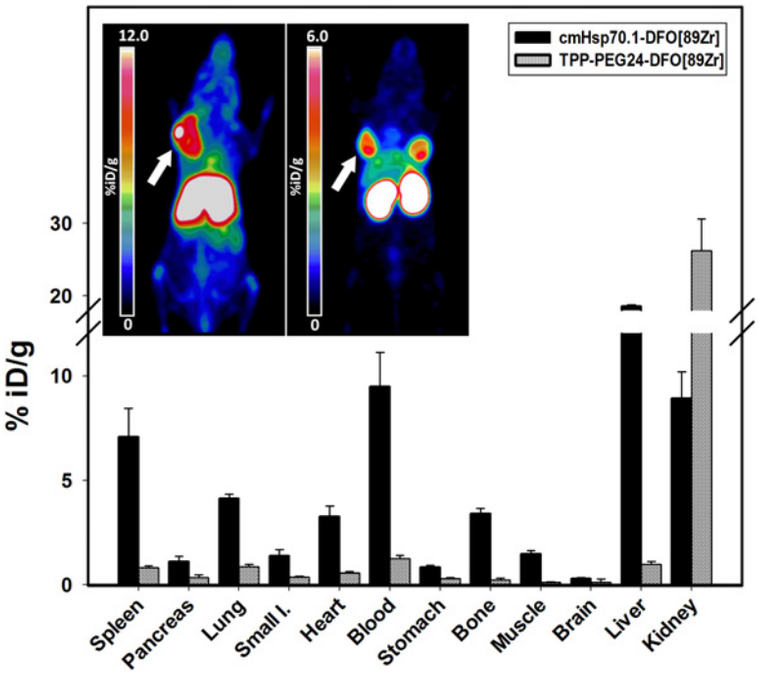

Figure 7.

Comparison of *in vivo* biodistribution of the Hsp70-reactive compounds cmHsp70.1-DFO[^{89}Zr] (MW = 150 kDa) and TPP-PEG$_{24}$-DFO[^{89}Zr] (MW = 3.5 kDa) in different organs (spleen, pancreas, lung, duodenum, heart, blood, stomach, bone, muscle, brain, liver, kidney) of 4T1 tumor-bearing mice following i.v. injection of 2.9 MBq and 4.4 MBq tracer equivalent, respectively. Inset, representative pseudocolor PET scans of cmHsp70.1-DFO[^{89}Zr] in a living mouse bearing subcutaneously implanted 4T1 wt tumor, 72 hours after intravenous administration (left), and of a mouse bearing subcutaneously implanted 4T1 (left shoulder) and CT26 (right neck) tumors, 24 hours after intravenous TPP-PEG$_{24}$-DFO[^{89}Zr] injection (right). Data are given in %ID/g tissue.

not negatively affected by PEGylation. The time for a complete internalization cycle of mHsp70, tagged either with TPP-[FITC] or TPP-PEG$_{24}$-[FITC], was determined as 3.2 and 1.3 minutes for 4T1 cells, respectively, and 0.5 and 2.5 minutes, respectively, for CT26 cells. These data reveal that the molecular weight of the tracer ranging from 1,975 g/mol (TPP-[FITC]) to 3,505 g/mol (TPP-PEG$_{24}$-[FITC]) did not show adverse effects on its internalization capacity. A comparison of the uptake kinetics of other membrane-bound target molecules, such as EGFR in HeLa cells (45), somatostatin receptor 2 (STR2) in CA20948 cells (46), or the chemokine receptor CXCR4 in 3T3 cells (47) revealed internalization cycles in the range of 10 to 20 minutes.

In vivo, the uptake capacity of TPP-PEG$_{24}$-DFO[^{89}Zr] tracer ranged from background level in mHsp70-negative benign fibroblast hyperplasia, over moderate (CT26 cells: 2.0 ± 0.4%ID/g) to high (4T1 cells: 5.47 ± 0.3%ID/g) and very high levels in mHsp70-overexpressing 4T1^{+} tumor cells (6.22 ± 1.1%ID/g). Biodistribution analysis further supports the capacity of TPP peptide as a tumor-specific tracer. Modification of TPP peptide by introducing a heterobifunctional PEG$_{24}$ moiety further improved the *in vivo* performance of the Hsp70-specific radiotracer by both, avoiding self-aggregation and prolonging the circulation time in the blood. While accumulation of the probe was already detectable during the first 6 hours after injection, specific tumor uptake with high contrast tumor-delineation became pronounced 9 hours after injection, and reached a maximum at 24 hours after administration of the TPP-based PET tracer. Moreover, according to the octanol-water partition coefficient measurements (log $P = -3.60 \pm 0.2$), the high hydrophilicity of the molecule, together with its small size, caused a significant kidney excretion and low accumulation in the liver (Fig. 6A). The presence of tracer accumulation in the gallbladder at early acquisition times (1–3 h) and the low accumulation in the liver at later time points indicates that the tracer is not primarily excreted via the hepatobiliary route. The pathway of elimination for the TPP-PEG$_{24}$-DFO[^{89}Zr] tracer is, in accordance to common knowledge (48), following the renal body clearance pathway of excretion of intravenously applied, small compounds. Therefore, TPP-based tracers also qualify for the delineation of small tumors and metastases in mHsp70-positive hepatocellular carcinoma and liver metastases (49). These entities are not addressable for compounds exceeding the size threshold for clearance through the hepatobiliary pathway. To further evaluate the dependency of the tracers' molecular size on the biodistribution, the performance of the TPP-peptide based tracer was compared with that of the mHsp70-targeting full-length murine IgG1 antibody-based tracer cmHsp70.1-DFO[^{89}Zr]. In contrast to the 3.5-kDa peptide tracer TPP-PEG$_{24}$-DFO[^{89}Zr] (K_d = 18.9 nmol/L), the 150 kDa cmHsp70.1-DFO[^{89}Zr] (K_d = 5.4 nmol/L) tracer is characterized by a high liver uptake and long blood half-life, which is characteristic for IgG antibodies. To improve the comparability of the biodistribution of the two compounds, circulation times with matching extravasation status were used to minimize falsifying effects of different tracer concentrations in the circulation. At 72 hours after intravenous injection of cmHsp70.1-DFO[^{89}Zr] and a circulation time of 24 hours for TPP-PEG$_{24}$-DFO[^{89}Zr], the extravasation status, represented by the blood-to-muscle ratios, were comparable for antibody and peptide (6.6 ± 1.4 and 6.4 ± 0.2, respectively). Apart from the high liver uptake of cmHsp70.1-DFO[^{89}Zr], the accumulation of the antibody-based tracer was also significantly higher ($P < 0.05$) in other healthy organs such as spleen, pancreas, lung, small intestine, heart, bone, and muscle compared with TPP-PEG$_{24}$-DFO[^{89}Zr]. Because the 3.5 kDa peptide-based tracer is excreted from the body via the renal pathway, this tracer enables the imaging of liver tumors and metastasizes. Although the uptake of cmHsp70.1-DFO[^{89}Zr], compared with the TPP-PEG$_{24}$-DFO[^{89}Zr] tracer, was higher in the tumor (13.4 ± 2.1%ID/g and 4.3 ± 0.7%ID/g, respectively), the tumor-specific contrast, as determined by the tumor-to-normal tissue ratios,

Published OnlineFirst September 18, 2018; DOI: 10.1158/0008-5472.CAN-18-0707

was favorable for the TPP peptide-based tracer (e.g., tumor-to-muscle ratio, antibody tracer: 10.3 ± 2.0, TPP-peptide tracer: 33.0 ± 1.1). In summary, due to unfavorable biodistribution kinetics caused by long blood circulation times and a slow tumor uptake, an significant accumulation in many healthy organs, particularly in the liver, which hampers the imaging of liver tumors and metastases, an increased the risk of radiotoxicity, and Fc receptor-mediated immunogenic off-target effects of full-length antibody-based tracers, the TPP-PEG_{24}-DFO[^{89}Zr] was developed as a PET tracer for future imaging applications in patients.

PET analysis revealed a maximum enrichment of TPP-based tracer, 24 hours after intravenous application, in different tumor types. This finding is in accordance with previously assessed data using a fluorescently labeled TPP probe (29). The continuous tracer accumulation in tumor cells over 24 hours may be explained in part by a backflush of the tracer from the kidneys into the blood stream. Because the fast internalization dynamics of mHsp70, recirculating TPP tracer can bind internalize into tumor cells with a fast kinetics.

Self-aggregation of the TPP-based tracer over time could be avoided by introducing a flexible 24-mer PEG chain (50). By future modifications of the PEG moiety length, reduction in kidney uptake will be approached, velocity of the tracer accumulation in the tumor could be further improved, while keeping the stability of the TPP peptide tracer.

Conclusion

A novel TPP-PEG_{24} based PET tracer provides a useful tool for exclusive targeting of malignant tumors of different entities. With its favorable tumor specificity and biodistribution, precise tumor delineation, absence of toxicity or immunogenicity, effortless synthesis and the successful proof-of-concept in preclinical models, it is expected that TPP peptide-based *in vivo* Hsp70 targeting will be a highly vibrant field in preclinical and clinical research in the near future.

Disclosure of Potential Conflicts of Interest

S. Stangl has ownership interest (including stock, patents, etc.) in a patent. M. Schwaiger is a consultant/advisory board member for GE Healthcare. G. Multhoff has ownership interest (including stock, patents, etc.) as a patent inventor. No potential conflicts of interest were disclosed by the other authors.

Authors' Contributions

Conception and design: S. Stangl, L. Tei, W. Sievert, M. Shevtsov, M. Schwaiger, C. D'Alessandria, G. Multhoff

Development of methodology: S. Stangl, L. Tei, J. Martinelli, W. Sievert, M. Shevtsov, M. Schwaiger, C. D'Alessandria, G. Multhoff

Acquisition of data (provided animals, acquired and managed patients, provided facilities, etc.): S. Stangl, L. Tei, F. De Rose, S. Reder, W. Sievert, M. Shevtsov, R. Rad, C. D'Alessandria, G. Multhoff

Analysis and interpretation of data (e.g., statistical analysis, biostatistics, computational analysis): S. Stangl, L. Tei, F. De Rose, J. Martinelli, W. Sievert, M. Shevtsov, C. D'Alessandria, G. Multhoff

Writing, review, and/or revision of the manuscript: S. Stangl, L. Tei, J. Martinelli, W. Sievert, M. Shevtsov, M. Schwaiger, C. D'Alessandria, G. Multhoff

Administrative, technical, or material support (i.e., reporting or organizing data, constructing databases): S. Stangl, W. Sievert, M. Shevtsov, R. Öllinger, G. Multhoff

Study supervision: S. Stangl, M. Shevtsov, C. D'Alessandria

Acknowledgments

The work was funded by the DFG (SFB 824/3, MAP, INST 411/37-1FUGG, INST 95/980-1FUGG, STA1520/1-1, DA1552/2-1), BMBF (01GU0823, 02NUK038A), BMWi (AiF), DKTK, and Alexander von Humboldt Fellowship granted to Maxim Shevtsov and Lorenzo Tei. The authors want to thank Martin Göttlicher and Kenji Schorpp for assistance with the MST measurements, Ramona Töppel for technical assistance, Markus Mittelhäuser for performing PET/CT measurements, and Christian Westiner for help with *in vitro* assays.

The costs of publication of this article were defrayed in part by the payment of page charges. This article must therefore be hereby marked *advertisement* in accordance with 18 U.S.C. Section 1734 solely to indicate this fact.

Received March 6, 2018; revised June 4, 2018; accepted September 14, 2018; published first September 18, 2018.

References

1. Sai KKS, Zachar Z, Bingham PM, Mintz A. Metabolic PET imaging in oncology. AJR Am J Roentgenol 2017;209:270–6.
2. Xu L, Josan JS, Vagner J, Caplan MR, Hruby VJ, Mash EA, et al. Heterobivalent ligands target cell-surface receptor combinations *in vivo*. Proc Natl Acad Sci U S A 2012;109:21295–300.
3. Weidle UH, Maisel D, Klostermann S, Schiller C, Weiss EH. Intracellular proteins displayed on the surface of tumor cells as targets for therapeutic intervention with antibody-related agents. Cancer Genomics Proteomics 2011;8:49–63.
4. Multhoff G, Botzler C, Wiesnet M, Muller E, Meier T, Wilmanns W, et al. A stress-inducible 72-kDa heat-shock protein (HSP72) is expressed on the surface of human tumor cells, but not on normal cells. Int J Cancer 1995;61:272–9.
5. Hartl FU, Bracher A, Hayer-Hartl M. Molecular chaperones in protein folding and proteostasis. Nature 2011;475:324–32.
6. Richter K, Haslbeck M, Buchner J. The heat shock response: life on the verge of death. Mol Cell 2010;40:253–66.
7. Mayer MP, Bukau B. Hsp70 chaperones: cellular functions and molecular mechanism. Cell Mol Life Sci 2005;62:670–84.
8. Calderwood SK, Ciocca DR. Heat shock proteins: stress proteins with Janus-like properties in cancer. Int J hyperthermia 2008;24:31–9.
9. Zorzi E, Bonvini P. Inducible hsp70 in the regulation of cancer cell survival: analysis of chaperone induction, expression and activity. Cancers 2011;3:3921–56.
10. Gabai VL, Yaglom JA, Waldman T, Sherman MY. Heat shock protein Hsp72 controls oncogene-induced senescence pathways in cancer cells. Mol Cell Biol 2009;29:559–69.
11. Gabai VL, Budagova KR, Sherman MY. Increased expression of the major heat shock protein Hsp72 in human prostate carcinoma cells is dispensable for their viability but confers resistance to a variety of anticancer agents. Oncogene 2005;24:3328–38.
12. Stangl S, Tontcheva N, Sievert W, Shevtsov M, Niu M, Schmid TE, et al. Heat shock protein 70 and tumor-infiltrating NK cells as prognostic indicators for patients with squamous cell carcinoma of the head and neck after radiochemotherapy: A multicentre retrospective study of the German Cancer Consortium Radiation Oncology Group (DKTK-ROG). Int J Cancer 2018;142:1911–25.
13. Bayer C, Liebhardt ME, Schmid TE, Trajkovic-Arsic M, Hube K, Specht HM, et al. Validation of heat shock protein 70 as a tumor-specific biomarker for monitoring the outcome of radiation therapy in tumor mouse models. Int J Radiat Oncol Biol Phys 2014;88:694–700.
14. Farkas B, Hantschel M, Magyarlaki M, Becker B, Scherer K, Landthaler M, et al. Heat shock protein 70 membrane expression and melanoma-associated marker phenotype in primary and metastatic melanoma. Melanoma Res 2003;13:147–52.
15. Ferrarini M, Heltai S, Zocchi MR, Rugarli C. Unusual expression and localization of heat-shock proteins in human tumor cells. Int J Cancer 1992;51:613–9.

Published OnlineFirst September 18, 2018; DOI: 10.1158/0008-5472.CAN-18-0707

16. Fujita Y, Nakanishi T, Miyamoto Y, Hiramatsu M, Mabuchi H, Miyamoto A, et al. Proteomics-based identification of autoantibody against heat shock protein 70 as a diagnostic marker in esophageal squamous cell carcinoma. Cancer Lett 2008;263:280–90.
17. Gehrmann M, Specht HM, Bayer C, Brandstetter M, Chizzali B, Duma M, et al. Hsp70–a biomarker for tumor detection and monitoring of outcome of radiation therapy in patients with squamous cell carcinoma of the head and neck. Radiat Oncol 2014;9:131.
18. Hantschel M, Pfister K, Jordan A, Scholz R, Andreesen R, Schmitz G, et al. Hsp70 plasma membrane expression on primary tumor biopsy material and bone marrow of leukemic patients. Cell Stress Chaperones 2000;5: 438–42.
19. Kleinjung T, Arndt O, Feldmann HJ, Bockmuhl U, Gehrmann M, Zilch T, et al. Heat shock protein 70 (Hsp70) membrane expression on head-and-neck cancer biopsy-a target for natural killer (NK) cells. Int J Radiat Oncol Biol Phys 2003;57:820–6.
20. Pfister K, Radons J, Busch R, Tidball JG, Pfeifer M, Freitag L, et al. Patient survival by Hsp70 membrane phenotype: association with different routes of metastasis. Cancer 2007;110:926–35.
21. Stangl S, Gehrmann M, Riegger J, Kuhs K, Riederer I, Sievert W, et al. Targeting membrane heat-shock protein 70 (Hsp70) on tumors by cmHsp70.1 antibody. Proc Natl Acad Sci U S A 2011;108:733–8.
22. Chames P, Van Regenmortel M, Weiss E, Baty D. Therapeutic antibodies: successes, limitations and hopes for the future. Br J Pharmacol 2009;157:220–33.
23. Anderson CJ, Connett JM, Schwarz SW, Rocque PA, Guo LW, Philpott GW, et al. Copper-64-labeled antibodies for PET imaging. J Nucl Med 1992;33:1685–91.
24. Holland JP, Divilov V, Bander NH, Smith-Jones PM, Larson SM, Lewis JS. 89Zr-DFO-J591 for immunoPET of prostate-specific membrane antigen expression in vivo. J Nucl Med 2010;51:1293–300.
25. Kamath AV. Translational pharmacokinetics and pharmacodynamics of monoclonal antibodies. Drug Discov Today Technol 2016;21–22: 75–83.
26. Kondo E, Saito K, Tashiro Y, Kamide K, Uno S, Furuya T, et al. Tumour lineage-homing cell-penetrating peptides as anticancer molecular delivery systems. Nat Commun 2012;3:951.
27. Gehrmann M, Stangl S, Kirschner A, Foulds GA, Sievert W, Doss BT, et al. Immunotherapeutic targeting of membrane Hsp70-expressing tumors using recombinant human granzyme B. PLoS One 2012;7:e41341.
28. Gehrmann M, Stangl S, Foulds GA, Oellinger R, Breuninger S, Rad R, et al. Tumor imaging and targeting potential of an Hsp70-derived 14-mer peptide. PLoS One 2014;9:e105344.
29. Stangl S, Varga J, Freysoldt B, Trajkovic-Arsic M, Siveke JT, Greten FR, et al. Selective *in vivo* imaging of syngeneic, spontaneous, and xenograft tumors using a novel tumor cell-specific hsp70 peptide-based probe. Cancer Res 2014;74:6903–12.
30. Zhang Y, Hong H, Cai W. PET tracers based on Zirconium-89. Curr Radiopharm 2011;4:131–9.
31. Francis GE, Delgado C, Fisher D, Malik F, Agrawal AK. Polyethylene glycol modification: relevance of improved methodology to tumour targeting. J Drug Target 1996;3:321–40.
32. Stangl S, Gehrmann M, Dressel R, Alves F, Dullin C, Themelis G, et al. In vivo imaging of CT26 mouse tumours by using cmHsp70.1 monoclonal antibody. J Cell Mol Med 2011;15:874–87.
33. Jerabek-Willemsen M, Wienken CJ, Braun D, Baaske P, Duhr S. Molecular interaction studies using microscale thermophoresis. Assay Drug Dev Technol 2011;9:342–53.
34. Wienken CJ, Baaske P, Rothbauer U, Braun D, Duhr S. Protein-binding assays in biological liquids using microscale thermophoresis. Nat Commun 2010;1:100.
35. Jacobson O, Zhu L, Niu G, Weiss ID, Szajek LP, Ma Y, et al. MicroPET imaging of integrin alphavbeta3 expressing tumors using 89Zr-RGD peptides. Mol Imaging Biol 2011;13:1224–33.
36. Renier N, Wu Z, Simon DJ, Yang J, Ariel P, Tessier-Lavigne M. iDISCO: a simple, rapid method to immunolabel large tissue samples for volume imaging. Cell 2014;159:896–910.
37. Bandyopadhyay A, Cambray S, Gao J. Fast diazaborine formation of semicarbazide enables facile labeling of bacterial pathogens. J Am Chem Soc 2017;139:871–8.
38. Cardoso F, Saghatchian M, Thompson A, Rutgers E, TRANSBIG Consortium Steering Committee. Inconsistent criteria used in American Society of Clinical Oncology 2007 update of recommendations for the use of tumor markers in breast cancer. J Clin Oncol 2008;26:2058–9; author reply 60–1.
39. Hosotani R, Kawaguchi M, Masui T, Koshiba T, Ida J, Fujimoto K, et al. Expression of integrin alphaVbeta3 in pancreatic carcinoma: relation to MMP-2 activation and lymph node metastasis. Pancreas 2002;25: e30–5.
40. McShane LM, Altman DG, Sauerbrei W, Taube SE, Gion M, Clark GM, et al. REporting recommendations for tumor MARKer prognostic studies (REMARK). Breast Cancer Res Treat 2006;100:229–35.
41. Lobo ED, Hansen RJ, Balthasar JP. Antibody pharmacokinetics and pharmacodynamics. J Pharm Sci 2004;93:2645–68.
42. El-Andaloussi S, Holm T, Langel U. Cell-penetrating peptides: mechanisms and applications. Curr Pharm Des 2005;11:3597–611.
43. Guo Z, Peng H, Kang J, Sun D. Cell-penetrating peptides: Possible transduction mechanisms and therapeutic applications. Biomed Rep 2016;4: 528–34.
44. Snyder EL, Dowdy SF. Cell penetrating peptides in drug delivery. Pharm Res 2004;21:389–93.
45. Roxrud I, Raiborg C, Pedersen NM, Stang E, Stenmark H. An endosomally localized isoform of Eps15 interacts with Hrs to mediate degradation of epidermal growth factor receptor. J Cell Biol 2008;180: 1205–18.
46. Chan HS, de Blois E, Morgenstern A, Bruchertseifer F, de Jong M, Breeman W, et al. *In vitro* comparison of 213Bi- and 177Lu-radiation for peptide receptor radionuclide therapy. PLoS One 2017;12:e0181473.
47. Boeck JM, Spencer JV. Effect of human cytomegalovirus (HCMV) US27 on CXCR4 receptor internalization measured by fluorogen-activating protein (FAP) biosensors. PLoS One 2017;12:e0172042.
48. Fleck C, Braunlich H. Factors determining the relationship between renal and hepatic excretion of xenobiotics. Arzneim-Forsch 1990;40: 942–6.
49. Li H, Sui C, Kong F, Zhang H, Liu J, Dong M. Expression of HSP70 and JNK-related proteins in human liver cancer: potential effects on clinical outcome. Dig Liver Dis 2007;39:663–70.
50. Hamidi M, Rafiei P, Azadi A. Designing PEGylated therapeutic molecules: advantages in ADMET properties. Expert Opin Drug Discov 2008;3:1293–307.

Published OnlineFirst September 18, 2018; DOI: 10.1158/0008-5472.CAN-18-0707

Cancer Research
The Journal of Cancer Research (1916–1930) | The American Journal of Cancer (1931–1940)

AACR American Association for Cancer Research

Preclinical Evaluation of the Hsp70 Peptide Tracer TPP-PEG$_{24}$-DFO[^{89}Zr] for Tumor-Specific PET/CT Imaging

Stefan Stangl, Lorenzo Tei, Francesco De Rose, et al.

Cancer Res 2018;78:6268-6281. Published OnlineFirst September 18, 2018.